Long-term variability in debris transiting white dwarfs

Amornrat Aungwerojwit [⬤],[1]★ Boris T. Gänsicke [⬤],[2,3] Vikram S. Dhillon [⬤],[4,5] Andrew Drake,[6] Keith Inight [⬤],[2] Thomas G. Kaye,[7] T. R. Marsh,[2] Ed Mullen,[8] Ingrid Pelisoli [⬤][2] and Andrew Swan [⬤][2]

[1]*Department of Physics, Faculty of Science, Naresuan University, Phitsanulok 65000, Thailand*
[2]*Department of Physics, University of Warwick, Coventry CV4 7AL, UK*
[3]*Centre for Exoplanets and Habitability, University of Warwick, Coventry CV4 7AL, UK*
[4]*Department of Physics and Astronomy, University of Sheffield, Sheffield S3 7RH, UK*
[5]*Instituto de Astrofísica de Canarias, E-38205 La Laguna, Tenerife, Spain*
[6]*Department of Astronomy, California Institute of Technology, 1200 E. California Boulevard, Pasadena, CA 91125, USA*
[7]*Foundation for Scientific Advancement, Sierra Vista, AZ 85650, USA*
[8]*Sycamore Canyon Observatory, Vail, AZ, USA*

ABSTRACT

Combining archival photometric observations from multiple large-area surveys spanning the past 17 years, we detect long-term variability in the light curves of ZTF J032833.52−121945.27 (ZTF J0328−1219), ZTF J092311.41+423634.16 (ZTF J0923+4236), and WD 1145+017, all known to exhibit transits from planetary debris. ZTF J0328−1219 showed an overall fading in brightness from 2011 through to 2015, with a maximum dimming of ≃0.3 mag, and still remains ≃0.1 mag fainter compared to 2006. We complement the analysis of the long-term behaviour of these systems with high-speed photometry. In the case of ZTF J0923+4236 and WD 1145+017, the time-series photometry exhibits vast variations in the level of transit activity, both in terms of numbers of transits, as well as their shapes and depths, and these variations correlate with the overall brightness of the systems. Inspecting the current known sample of white dwarfs with transiting debris, we estimate that similar photometric signatures may be detectable in one in a few hundred of all white dwarfs. Accounting for the highly aligned geometry required to detect transits, our estimates imply that a substantial fraction of all white dwarfs exhibiting photospheric metal pollution from accreted debris host close-in planetesimals that are currently undergoing disintegration.

Key words: minor planets, asteroids: general – planets and satellites: physical evolution – planetary systems – white dwarfs.

1 INTRODUCTION

Practically all known planet hosts will evolve eventually into white dwarfs, and large parts of the various components of their planetary systems – planets, moons, asteroids, and comets will survive that metamorphosis (Sackmann, Boothroyd & Kraemer 1993; Mustill & Villaver 2012; Adams, Anderson & Bloch 2013; Veras, Shannon & Gänsicke 2014b; Payne et al. 2016; Caiazzo & Heyl 2017; Mustill et al. 2018; Martin et al. 2020; Maldonado et al. 2021). Rich observational evidence for such evolved planetary systems at white dwarfs exists in the form of photospheric contamination from the accretion of planetary debris (Zuckerman et al. 2003; Koester, Gänsicke & Farihi 2014), infrared excess and metallic emission lines from compact dusty and gaseous debris discs (Zuckerman & Becklin 1987; Gänsicke et al. 2006), transits from both debris (Vanderburg et al. 2015; Vanderbosch et al. 2020) and planets (Vanderburg et al. 2020), and spectroscopic detections of planetesimals (Manser et al. 2019), and giant planets (Gänsicke et al. 2019; Schreiber et al. 2019).

Among all those features, white dwarfs accreting the debris of tidally disrupted rocky bodies (Debes & Sigurdsson 2002; Jura

2003) are most common-place. Yet, our understanding of the full sequence of the processes involved is still limited, beginning with the gravitational scattering of these bodies onto orbits that take them into the tidal disruption radius of the white dwarf (Bonsor & Wyatt 2012; Frewen & Hansen 2014; Stephan, Naoz & Zuckerman 2017; Smallwood et al. 2018; Antoniadou & Veras 2019), the actual disruption and subsequent circularization of the debris into a compact circumstellar disc (Debes et al. 2012; Veras et al. 2014a, 2015; Brown, Veras & Gänsicke 2017; Malamud & Perets 2020a), and the further evolution of these discs (Metzger, Rafikov & Bochkarev 2012; Kenyon & Bromley 2017a, b; Miranda & Rafikov 2018). Although observational estimates of the disc life times are ∼10^4–10^6 yr (Girven et al. 2012; Cunningham et al. 2021), there is growing evidence of variability in the optical (Wilson et al. 2014; Manser et al. 2016; Dennihy et al. 2018; Gänsicke et al. 2018; Gentile Fusillo et al. 2021), and infrared emission from these discs (Xu & Jura 2014; Xu et al. 2018b; Swan, Farihi & Wilson 2019; Swan et al. 2020), that these discs are not static systems, but dynamically active.

The first genuine signature of an ongoing disruption event was the discovery of multiple transits from debris at WD 1145+017 with orbital periods of ≃4.5 h (Vanderburg et al. 2015), consistent with quasi-circular orbits (Gurri, Veras & Gänsicke 2017; Veras et al. 2017) near the tidal disruption radius for a rocky body. The system

★ E-mail: amornrata@nu.ac.th

also exhibits strong photospheric metal contamination as well as infrared excess and gaseous absorption lines from the circumstellar debris (Vanderburg et al. 2015; Xu et al. 2016; Fortin-Archambault, Dufour & Xu 2020) – as such, WD 1145+017 was the textbook example that confirmed the general framework initially laid out by Jura (2003). Intense monitoring of WD 1145+017 since its discovery shows that the amount of occulting debris varies dramatically on time-scales of months to years, demonstrating the ongoing dynamic activity within the system (Gänsicke et al. 2016; Gary et al. 2017; Rappaport et al. 2018).

In stark contrast, the debris transits in ZTF J013906.17+524536.89 (hereafter ZTF J0139+5245), the second system discovered, recur every ≃107 d (Vanderbosch et al. 2020), highlighting that the tidal disruption processes are likely to be more complex (Veras, McDonald & Makarov 2020; Malamud & Perets 2020b), or that indeed thermal destruction could play a key role (Shestakova & Serebryanskiy 2023).

Guidry et al. (2020) announced the identification of five additional systems that were good candidates for displaying debris transits. One of these, ZTF J032833.52−121945.27 (hereafter ZTF J0328−1219) has been followed up in more detail by Vanderbosch et al. (2021), who identified two orbital periods, 9.94 and 11.2 h. Finally, Farihi et al. (2022) discovered debris transits with an orbital period of 25 h in WD 1054−226. It is now clear that actively disintegrating planetesimals can be found spanning a wide range in orbital parameters, and levels of dynamical activity.

Whereas ongoing searches for additional systems will further map out the parameter space of orbital periods, eccentricities, and multiplicity of the fragments causing the transits, it is equally important to better characterize the eight systems identified so far, in particular to explore the evolution of their debris. Here, we make use of the data from large-area photometric surveys and detailed time-series photometry to investigate the long-term variability and the changes in transit activity and morphology of three white dwarfs with debris transits: ZTF J0328−1219, ZTF J0923+4236, and WD 1145+017.

2 OBSERVATIONS

2.1 Time-domain surveys

We retrieved the sparse, long-term photometry of ZTF J0328−1219, ZTF J0923+4236, and WD 1145+017 from the following wide-field time-domain surveys (Table 1).

2.1.1 Catalina real time transient survey

The Catalina Real Time Transient Survey (CRTS; Drake et al. 2009) uses filter-less photometry obtained with three telescopes: the Catalina Sky Survey telescope (CSS, 0.7 m aperture, covering Dec = −25° to +70°, Larson et al. 2003), the Mt. Lemmon Survey telescope (MLS, 1.5 m aperture, covering Dec = −5° to +5°), and the Siding Springs Survey telescope (SSS, 0.5 m aperture, covering Dec = −80° to 0°). The survey strategy was optimized for the detection of near-Earth objects, obtaining typically four 30 s exposures per night, with limiting magnitudes of $V \simeq$ 19.0, 19.5, 21.5 for the SSS, CSS, and MLS observations. Object detection and aperture-based photometry were obtained using the SExtractor (Bertin & Arnouts 1996) package. A public data base[1] provides access to observations obtained between

Table 1. Summary of the time-domain survey photometry used for the analysis of the three white dwarfs exhibiting transits from circumstellar debris.

Star	Survey	Date range	Filter	Epochs
ZTF J0328−1219	CRTS	2005-12-01 to 2015-12-02	Clear	293
	ASAS-SN	2012-01-29 to 2018-11-29	*V*	551
	ASAS-SN	2017-09-16 to 2023-08-11	*g*	2030
	ATLAS	2015-10-02 to 2023-08-14	*o*	2565
	ATLAS	2015-08-09 to 2023-08-15	*c*	709
	ZTF	2017-12-20 to 2023-02-16	*g*	363
	ZTF	2017-11-16 to 2023-02-19	*r*	375
ZTF J0923+4236	CRTS	2005-12-08 to 2016-04-18	Clear	486
	ASAS-SN	2012-10-22 to 2018-04-12	*V*	68
	ASAS-SN	2017-10-29 to 2023-06-15	*g*	598
	ATLAS	2015-10-05 to 2023-06-05	*o*	2036
	ATLAS	2015-10-21 to 2023-06-09	*c*	573
	ZTF	2017-12-20 to 2023-05-01	*g*	617
	ZTF	2017-10-28 to 2023-05-01	*r*	832
WD 1145+017	CRTS	2005-12-02 to 2016-05-09	Clear	771
	ASAS-SN	2012-02-16 to 2018-11-13	*V*	285
	ASAS-SN	2017-11-30 to 2023-07-16	*g*	1403
	ATLAS	2016-01-21 to 2023-07-30	*o*	1795
	ATLAS	2016-01-13 to 2023-06-16	*c*	580
	ZTF	2017-12-19 to 2023-04-30	*g*	227
	ZTF	2017-12-03 to 2023-04-29	*r*	341

2005 and 2014. We used a CRTS-internal data base that provides additional observations until May 2016.

2.1.2 All-Sky Automated Survey for Supernovae

The All-Sky Automated Survey for Supernovae (ASAS-SN; Shappee et al. 2014; Kochanek et al. 2017) consists of a global network of 0.14 m telescopes obtaining nightly all-sky photometry, using *V*- and *g*-band filters, with a limiting magnitude of $V \simeq$ 17–18 mag. Each ASAS-SN epoch consists of three dithered 90 s exposures. We retrieved the ASAS-SN light curves via positional queries using the aperture photometry service provided by the SkyPatrol.[2] We only included detections in our analysis, i.e. excluded epochs that only provided an upper limit on the brightness of our targets.

2.1.3 Asteroid Terrestrial-impact Last Alert System

The Asteroid Terrestrial-impact Last Alert System (ATLAS; Tonry et al. 2018; Smith et al. 2020) uses a global network of 0.5 m telescopes to provide nightly (−50° < Dec < +50°) or bi-nightly (in the polar regions) photometry using broad-band cyan (*c*-band) and orange (*o*-band) filters. The data is obtained as four 30 s exposures spaced out over about an hour to maximize the efficiency for detecting near-Earth asteroids. We obtained the ATLAS light curves by using the forced photometry service,[3] including proper-motions from *Gaia* Data Release 3 (Gaia Collaboration et al. 2020). We only included in our analysis detections with photometric uncertainties <0.1 mag.

2.1.4 Zwicky Transient Factory

The Zwicky Transient Factory (ZTF; Bellm et al. 2019; Masci et al. 2019) uses the 48 inch (1.2 m) Palomar telescope, taking 30 s exposures primarily in the *g*- and *r*-bands, with less frequent observation in the *i*-band, with a typical limiting magnitude of $r \simeq$ 20.5–21.0 mag. ZTF carries out multiple surveys in parallel: the public surveys

---

[1] http://nesssi.cacr.caltech.edu/DataRelease/

[2] https://asas-sn.osu.edu/
[3] https://fallingstar-data.com/forcedphot/
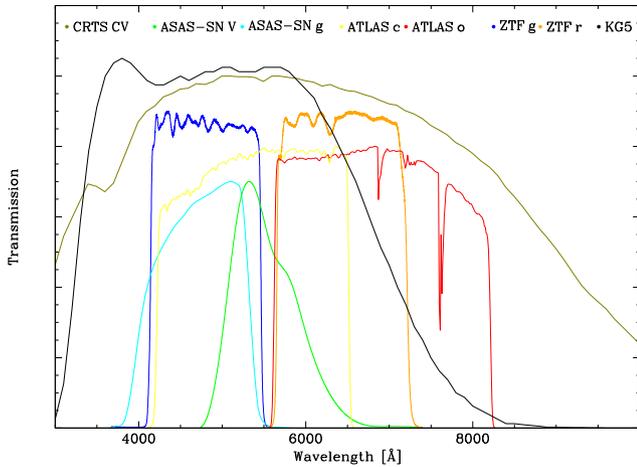
Figure 1. The transmission curves of the photometric surveys used for this study. The transmission curves for CRTS, ZTF, and ATLAS were retrieved from the Spanish Virtual Observatory filter service (Rodrigo & Solano 2020) apart from the KG5 filter, which was obtained from the HiPERCAM/ULTRACAM/ULTRASPEC filter data base[4]. For the ASAS-SN filters, we show representative *V*- and *g*-band curves. The curves have been scaled vertically for clarity, i.e. are not reflective of the absolute transmission of the different surveys.

re-visit the Northern sky every three days and the Galactic plane every day, and private surveys are used for other experiments, such as observing dedicated fields several times per night for transient searches. We retrieved the *g*- and *r*-band PSF photometry within ZTF Data Release 19 from the Infrared Science Archive (IRSA) service, using the recommended BAD_CATFLAGS_MASK = 32768 bitmask to filter out bad quality data.

2.1.5 Survey cross-calibration

Our goal was to use all available survey data to establish the long-term light curves of the three debris-transiting systems, which requires to account for the offsets between the different filter band passes (Fig. 1). For that purpose, we selected single white dwarfs from the catalogue of Gentile Fusillo et al. (2021), which have Pan-STARRS1 (Chambers et al. 2016) *g*–*i* colours as close as possible to those of the transiting systems, and retrieved their survey data as well. We then computed the median magnitudes of the reference white dwarfs across all six filter band passes, and scaled the CRTS, ASAS-SN, ATLAS, and ZTF *r*-band data to match the median magnitude of the ZTF *g*-band data. The resulting scaled long-term light curve for WD J153210.05+135616.11 (WD J1532+1356, also known as GD 184) is shown in Fig. 2. Checking the survey data of other white dwarfs with nearly identical *g*–*i* colours, and using them as mutual reference stars, we established that they were non-variable. We found that this approach works robustly with the exception of the ASAS-SN *V*- and *g*-band data, which can show residual offsets with respect to the other surveys of $\simeq\pm0.1$ mag. Despite various investigations, we were unable to unambiguously identify the source of these offsets. We note that the targets of our study are near the faint limit of ASAS-SN, and that data for an individual system is taken at multiple telescopes. Slight differences in the response functions of the different telescopes or the treatment of sky

background and scattered light may contribute to the small offsets we found. We adopted WDJ 145452.89+084640.44 as reference star for WD 1145+017, and given the large-amplitude variability of ZTF J0923+4236, we decided to use scale the median magnitudes of that system itself to that of its ZTF *g*-band data.

One caveat in the interpretation of variability detected in the joint-up survey photometry is that white dwarfs exhibiting transits caused by planetary debris might change both in brightness and colour, which would indeed be expected if a fraction of the circumstellar material is in the form of micro-metre sized dust. Simultaneous multi-wavelength studies of WD 1145+017 concluded that the transit depths did not show noticeable changes across the optical to infrared wavelength ranges (Zhou et al. 2016; Croll et al. 2017; Xu et al. 2018a, 2019). However, Hallakoun et al. (2017) reported *shallower* transits at shorter wavelengths ($u - r \simeq -0.05$ mag) in WD 1145+017. The authors suggested that this 'blueing' is related to a reduction in the strength of absorption lines from circumstellar gas during the transits (see also Izquierdo et al. 2018). Given that most of the photometry discussed here does not cover wavelengths <4000 Å, where the majority of strong metal absorption lines are located, the effect of circumstellar gas should not strongly affect our analysis.

2.2 ULTRASPEC fast photometry

During 2016–2023, we obtained high-speed photometry of ZTF J0328−1219, ZTF J0923+4236, and WD 1145+017 using the frame-transfer camera ULTRASPEC (Dhillon et al. 2014) mounted on the 2.4-m Thai National Telescope (TNT) on Doi Inthanon. We used a KG5 short-pass filter that cuts off red light beyond 7000 Å, and exposure times varying between 3.0 and 10.0 s, depending on the brightness of the objects and the observing conditions, with less than 15 ms dead time. The details of observations are provided in Table 2. All data sets were reduced using HiPERCAM data reduction pipeline.[5] The light curves of these ZTF J0328−1219, ZTF J0923+4236, and WD 1145+017 are shown in Figs 4, 7, and 9, respectively.

We normalized each TNT light curve by computing the median flux of the 50 brightest data points, and setting that flux level to unity, and report the average transmission with respect to that level for each light curve in Table 2. In cases where light curves exhibit clean out-of-transit stretches, this definition would allow a measurement of average absorption by the transits; however, as we will see later, in many cases, the TNT light curves show continuously varying levels of flux, and hence our normalisation is only relative to the brightest moments captured by a given light curve.

2.3 Liverpool telescope

We obtained sparse photometry of ZTF J0923+4236 with the Liverpool Telescope (LT) from 2020 December 19 to 2021 January 13, using the IO:O camera. We used the Bessel *B*-band filter, which provides high throughput over the range $\simeq$3800–4900 Å and the default detector binning of 2 × 2. We collected a total of 88 60 s images. The LT data are provided in a reduced (bias-corrected and flat-fielded) format, and we extracted the photometry of ZTF J0923+4236 using the pipeline of Gänsicke et al. (2004).

---

[4] http://www.vikdhillon.staff.shef.ac.uk/ultracam/filters/filters.html

[5] https://github.com/HiPERCAM/hipercam
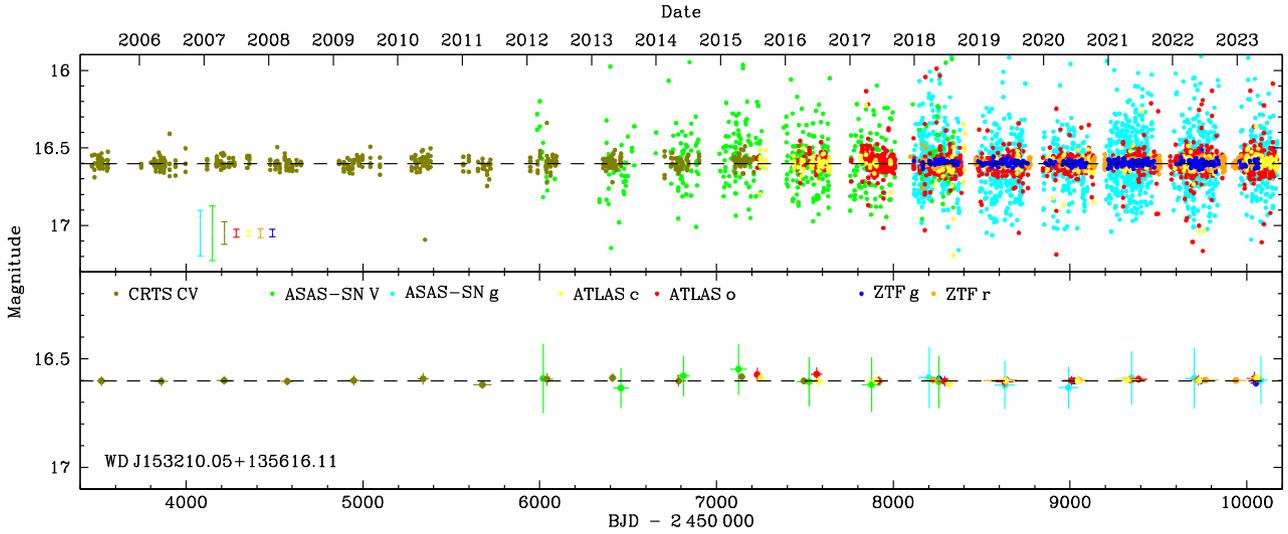
Figure 2. Long-term light curve of the white dwarf WD J153210.05+135616.11, which we used as reference star for ZTF J0328−1219. The individual observations are shown in the top panel. Median uncertainties of the individual measurements are displayed for each of the survey band passes in the lower left corner. The light curves of the different surveys have been offset such that their median magnitudes match that of the ZTF *g*-band data. The bottom panel shows the seasonal averages for each survey. The dashed lines in the bottom and top panels indicate the median brightness computed from the individual CRTS measurements obtained during the first two seasons (2006–2007). For this non-variable white dwarf, the seasonal averages agree within their respective uncertainties.

Table 2. Log of the TNT photometric observations, Exp. is the exposure time, Mag. the magnitude in the KG5 filter, and Trans. the average transmission.

Date	UT	Filter	Exp. (s)	Frames	Mag.	Trans.
ZTF J0328−1219						
2020 Dec 23	12:09-18:11	KG5	3.0	4621	17.08	0.91
2020 Dec 24	11:53-18:10	KG5	3.0	5536	17.03	0.92
2021 Dec 01	13:08-19:57	KG5	5.0	4030	16.99	0.92
ZTF J0923+4236						
2020 Dec 23	18:53-23:18	KG5	7.0	1908	18.04	0.88
2020 Dec 24	18:21-23:17	KG5	7.0	2026	18.02	0.87
2021 Mar 12	12:20-19:37	KG5	10.0	2328	17.90	0.90
2021 Mar 13	12:25-19:43	KG5	10.0	2236	17.89	0.92
2022 Mar 27	13:58-19:28	KG5	7.0	2466	17.85	0.93
2022 Mar 30	14:17-18:24	KG5	7.0	1835	17.84	0.89
WD 1145+017						
2016 Jan 18	17:14-23:13	KG5	3.0	3325	17.57	0.81
2016 Feb 10	17:38-23:06	KG5	3.0	3089	17.52	0.80
2017 Feb 08	18:17-23:10	KG5	3.0	4815	17.53	0.85
2017 Mar 02	17:52-22:58	KG5	3.0	4893	17.56	0.87
2018 Feb 24	14:52-19:53	KG5	3.0	4920	17.51	0.88
2019 Feb 04	18:38-23:16	KG5	3.0	4546	17.41	0.94
2020 Jan 09	17:54-23:20	KG5	5.0	3443	17.43	0.89
2021 Feb 22	18:40-23:01	KG5	5.0	2682	17.49	0.93
2022 Mar 26	14:36-21:05	KG5	5.0	4072	17.45	0.95
2023 Feb 20	16:28-21:50	KG5	6.2	2787	17.47	0.94

2.4 Time-series monitoring of WD 1145+017

Intense time-series photometric observations of WD 1145+017 have been obtained since the discovery of transits in 2015 using a range of observatories. We report here the average transmission measured from individual light curves obtained at Hereford Arizona Observatory (HAO) using a 16 arcsec telescope (see Rappaport et al. 2016 for details), at Sycamore Canyon Observatory (SCO) using a 20 arcsec telescope, and at Raemor Vista Observatory (RVO)

using a 1.1 m fully automated Dahl-Kirkam with an Apogee camera equipped with a back-illuminated E2V chip. Exposure times were typically in the range 30–60 s and the SCO and RVO data were reduced in a standard fashion using the AstroimageJ software.

3 RESULTS

3.1 ZTF J032833.52−121945.27

ZTF J0328−1219 was discovered as a white dwarf exhibiting transits of circumstellar debris by Guidry et al. (2020), and the subsequent analysis of *TESS* and ground-based photometry by Vanderbosch et al. (2021) led to the identification of two periodic signals, 9.34 and 11.2 h, which the authors interpreted as the orbital periods of debris fragments.

The CRTS light curve of ZTF J032−1219 (Fig. 3), which exhibits gaps due to the seasonal visibility of the star, displays a slight dimming beginning in ≃2011. The seasonal average brightness continued to drop in the following years, ending up ≃0.3 mag fainter in 2014, compared to the first season in 2006, after which CRTS recorded the system brightening again. The reference star, WD J1532+1356, shows a constant brightness across the 17 years of survey coverage, with consistent seasonal averages across the different surveys (Fig. 2). As an additional check, we investigated the possibility of the long-term brightness variation seen in the CRTS data of ZTF J0328−1219 being related to instrumental effects by extracting the CRTS light curves of three nearby (<1.5 arcmin) stars, i.e. which were observed in the same field as ZTF J0328−1219. The light curves of these stars remain constant in brightness throughout the operations of CRTS, confirming that the dimming of ZTF J0328−1219 is intrinsic to the system. This faint state is confirmed independently by the first seasons of the ASAS-SN *V*-band data, which then shows the brightness of ZTF J0328−1219 to recover. Throughout the years 2016 to 2023, ZTF, ASAS-SN, and ZTF show the system at nearly constant
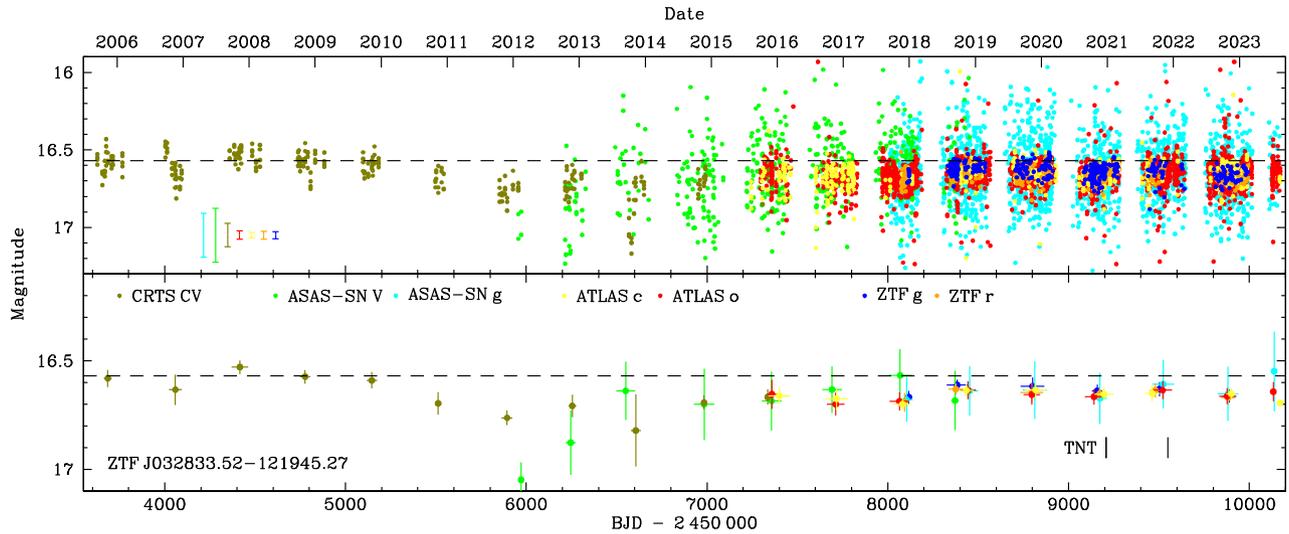
Figure 3. Long-term light curve of ZTF J0328−1219, all symbols have the same meaning as in Fig. 2. We have used WD J153210.05+135616.11 as reference star to compute offsets between the different surveys. The CRTS data show that the system began to gradually dim around 2011, reaching a minimum brightness around 2013 to 2014, after which it recovered in brightness, though, not quite reaching the level of the early CRTS seasons. The times at which we obtained TNT/ULTRASPEC photometry are indicated by tick-marks in the bottom panel, the corresponding light curves are shown in Fig. 4.
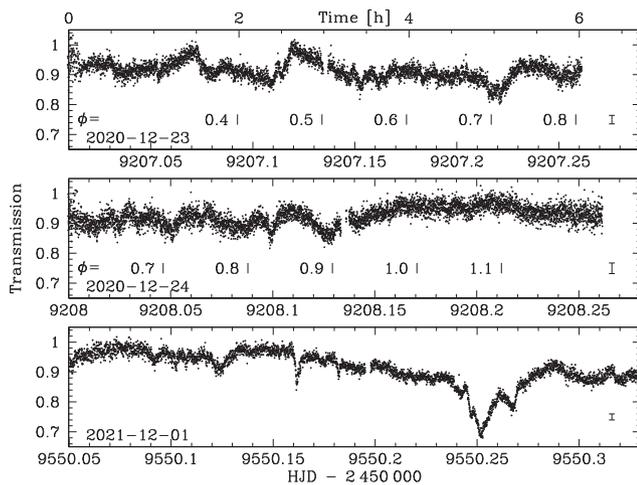
Figure 4. TNT light curves of ZTF 0328−1219 displaying both sharp, narrow transits, and broader, more complex structured absorption features. The median values of the photometric uncertainties are illustrated by the error bar in the bottom-right of each panel. Note that each observing run is shorter than the likely orbital periods detected by Vanderbosch et al. (2021), 9.94 and 11.2 h. We computed orbital phases for the light curves shown in the top two panels, using the ephemeris of the 9.94 h period given by Vanderbosch et al. (2021), see their fig. 2 (their ephemeris is too uncertain to be applied to our 2021 December 1 data shown in the bottom panel). Orbital phases are labelled and indicated by tick marks below the light curves. The morphology of the light curve undergoes changes over a small number of cycles, possibly due to the beat with the secondary period of 11.2 h or intrinsic variability. Nevertheless, some structures are reminiscent to those seen in the light curves of Vanderbosch et al. (2021), taken between 2020 December 12 and 15, e.g. the dip at $\phi \simeq 0.7$ and the broad minimum near $\phi \simeq 0.9$.

magnitude, with consistent seasonal magnitudes across the different surveys.

Noticeable is a large discrepancy between the seasonal averages of the CRTS and ASAS-SN V-band data in the three years where they overlap, 2012−2014. Given the sparse sampling of CRTS and ASAS-SN in 2012 and 2014 (in particular the first season of ASAS-SN V-band data, which only had four measurements), it is possible that the two surveys caught ZTF J0328−1219 in different states and/or different phases of the transiting debris. We note that the offsets determined from WD J1532+1356 may not be correct if the colour of ZTF J0328−1219 changes substantially with time, e.g. due to the production and subsequent dissipation of large amounts of small dust particles.

Our TNT light curves (Fig. 4) resemble those obtained by Vanderbosch et al. (2021) (their fig. 2). Similar to the TNT light curves of WD 1145+017 (e.g. fig. 1 in Gänsicke et al. 2016), ZTF J0328−1219 displays a mix of narrow, well-defined transit features and broader, complex absorption structures, with no constant 'out-of-transit' stretch. As such, it is conceivable that the flux from the white dwarf is attenuated *at all orbital phases*, and hence the star is dimmed overall with respect to its intrinsic brightness, which would be consistent with the fact that the latest long-term photometric data shows the brightness level of ZTF J0328−1219 still ≃0.1 mag fainter than during the earliest available survey data. This hypothesis would suggest that the transit activity, in terms of depth and/or number, was much higher during the 2011–2015 fading event. We analysed the CRTS and ASAS-SN V-band data obtained during those years using an Analysis-of-Variance (AoV) method (Schwarzenberg-Czerny 1996), but did not detect and periodic signal. Analysing the data from 2018 on-wards, we do detect the orbital period of 9.93 h reported by Vanderbosch et al. (2021). The absence of a periodic signal during the dimming event may be the result of the sparse sampling of the CRTS and ASAS-SN V-band data, and/or relatively rapid evolution of the orbital period(s) of the debris causing the dimming.

3.2 ZTF J092311.41+423634.16

ZTF J0923+4236 was identified by Guidry et al. (2020) as a white dwarf exhibiting irregular transits with complex structures in its ZTF light curve. A limited amount of fast photometry obtained by Guidry et al. (2020) revealed smooth, low-amplitude (≃0.1 mag)
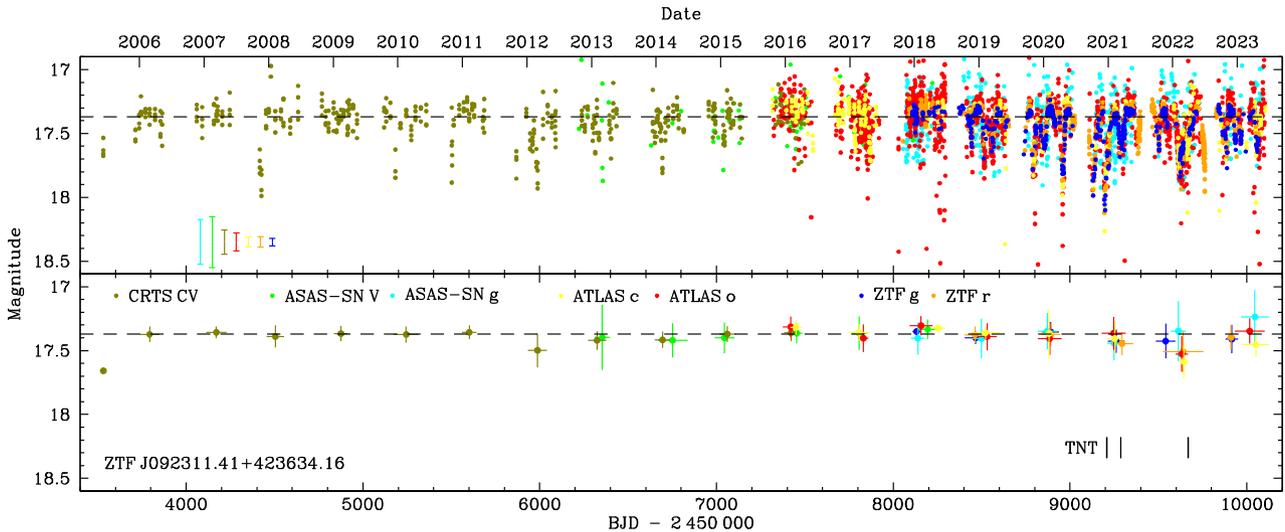
Figure 5. Long-term light curve of ZTF J0923+4236, all symbols have the same meaning as in Fig. 2. Given the large-amplitude variability, the photometry of the different surveys was offset by their median values relative to the ZTF *g*-band data. It is apparent that the system has been undergoing deep ($\simeq 1$ mag) fading events over the past $\simeq 17$ yr, which typically last a few months, see Fig. 6 for a zoom-in on several of these events. Even though not strictly periodic, these events are sufficiently regular not to affect the seasonal median brightness of the system. In contrast to ZTF J0328−1219 (Fig. 3), the seasonal magnitude of ZTF J0923+4236 has remained, within uncertainties, at a steady level, with the exception of the 2022/2023, where more scatter between the different surveys is seen.
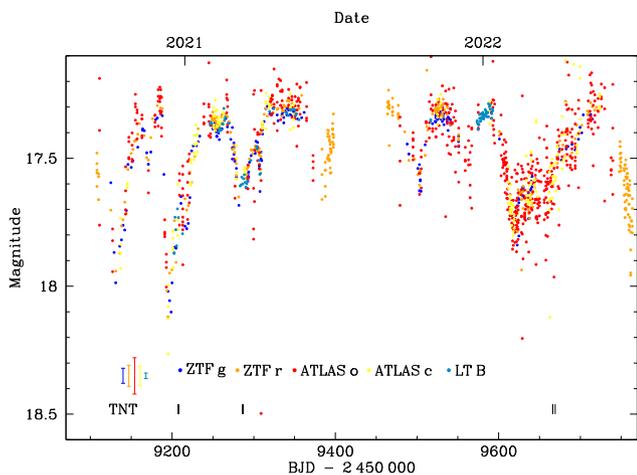
Figure 6. Zoom-in of the long-term light curve of ZTF 0923+4236, all symbols have the same meaning as in Fig. 2, with the addition of observations obtained with the LT.

variability with a time-scale of $\simeq 1$ h. The authors classified the star from low-resolution spectroscopy as having a hydrogen-dominated (DA) atmosphere.

The extended long-term light curve of ZTF J0923+4236 (Figs 5 and 6 for a zoom-in) demonstrates that the system has been undergoing fading events on time-scales of months, with an amplitude of up to $\simeq 1$ mag over the past 17 years. The seasonal average magnitudes remain broadly constant throughout the extended photometric coverage. We subjected the combined long-term light curve to an AoV analysis, but the only long-period signal detected is the lunar cycle.

We obtained the first TNT data of ZTF J0923+4236 in December 2020, when the system was near its faintest state (see Fig. 6), and the light curves display rapid variability on time-scales of a few minutes (Fig. 7). We analysed both nights separately, and whereas the AoV

power spectra show multiple signals in the range of $\simeq 10$ min to $\simeq 1$ h, none of these signals appear in both nights, and we conclude that the observations contain no evidence for a periodic signal. Overall, these TNT light curves are reminiscent of the transiting WD 1054−226 (Farihi et al. 2022, e.g. their Figs 2 and 6), though with variability occurring on even shorter time-scales in ZTF J0923+4236. It is important to keep in mind that transiting debris can only result in dimming, not in brightening. Hence, the true flux level of the unobscured white dwarf is likely to be higher than the brightest segments of these two light curves, i.e. absorption by transiting debris blocks some amount of the white dwarf flux at all orbital phases.

When we re-visited ZTF J0923+4236 in March 2021, the system was in a slightly brighter state, and the two TNT light curves are totally devoid of any transit activity. Further observations obtained in March 2022, again at an intermediate brightness level, show mild variability on time-scales of $\simeq 1$ h, similar to the light curves shown by Guidry et al. (2020) (their fig. 10), which faded away in our last observation.

Whereas the larger transit activity observed in December 2020 will result in an overall dimming of the average brightness of the white dwarf, the long-term light curve (Fig. 6) shows an overall fading of nearly one magnitude, larger than the maximum depth of $\simeq 20$ per cent observed on short time-scales within the TNT light curves. It thus appears that the transit activity correlates with an overall dimming of the system. The absence of a periodicity in the long-term variability is very puzzling, as a debris stream on an eccentric orbit would result in periodic dimming, as observed every $\simeq 107$ d in ZTF J0139+5245 (Vanderbosch et al. 2020).

3.3 WD 1145+017

WD 1145+017 is the prototype of white dwarfs exhibiting debris transits, discovered by Vanderburg et al. (2015) using *K2* data. Vanderburg et al. (2015) determined a dominant orbital period of 4.49 h and additional signals at slightly shorter orbital periods. The
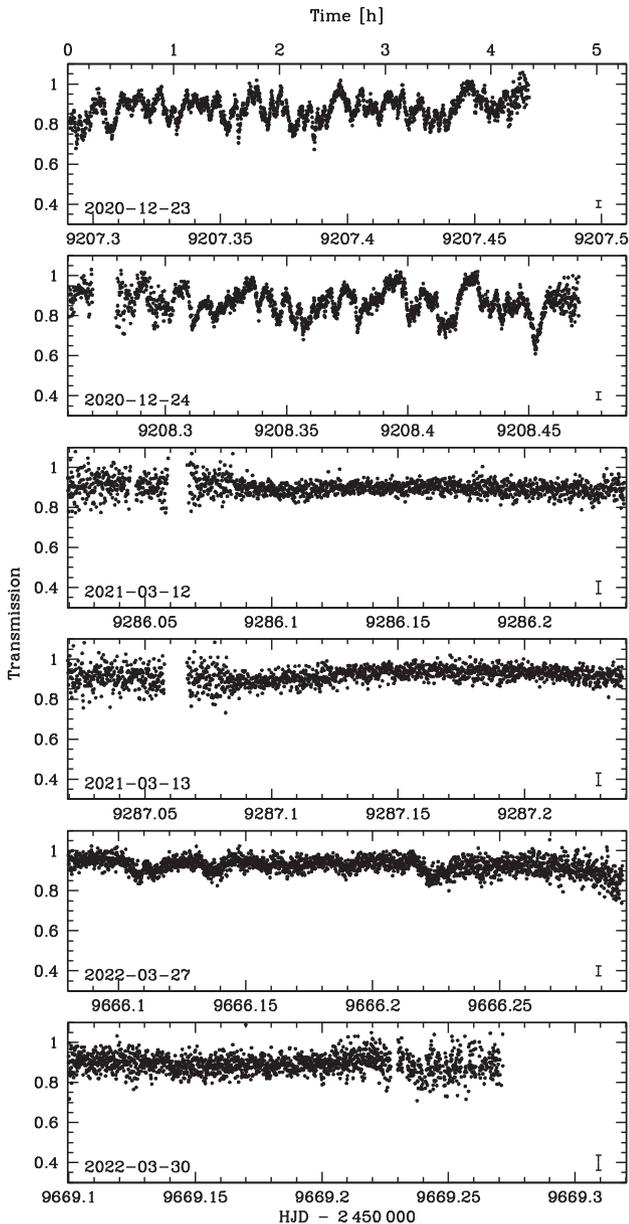
Figure 7. TNT light curves of ZTF 0923+4236. The transit activity appears to be correlated with the overall brightness, the light curves in the top two panels were obtained near the faintest state of the system (Fig. 6), in contrast, the middle two light curves were obtained during an intermediate brightness state. The slight modulation in the 2021 March 13 light curve likely arises from an imperfect extinction correction. The median values of the photometric uncertainties are illustrated by the error bar in the bottom-right of each panel.

Figure 8. Long-term averages of the orbital transmission of WD 1145+017, derived from intense photometric monitoring of the system using the facilities as described by Gary et al. (2017).

system from December 2015 throughout July 2016. The authors defined a photometric equivalent width as the orbital average of the transit absorption, and showed (their figs 9 and 10) that this measure increased from a fraction of a per cent during the *K2* observations to reaching nearly ten per cent in 2016, with large fluctuations on time-scales of months.

Here, we present an update of the analysis of Gary et al. (2017), including additional observations from mid-2016 to July 2023. We use here a slightly different definition, showing the data as transmission, which is essentially one minus the equivalent width defined by Gary et al. (2017). The new data (Fig. 8) shows that the overall transit activity reached a maximum around 2017, with the average transmission dropping almost to 80 per cent. In the following years, the transit activity decreased, with the average transmission varying from 2019 to 2021 between close to zero and five per cent. After that, the average transmission remained at very high levels of about one per cent.

We have obtained fast TNT photometry of WD 1145+017 from November 2015 throughout April 2023, which illustrates the change in the transit activity of the system, both in terms of morphology of the individual transits and the overall light curve (Fig. 9). During very active periods (2016 to 2017), there is hardly any segment of the light curve that is not affected by transits, with the implication that the orbital average transmission derived from these data should be considered a lower limit. In 2018 and 2019, the deep and sharp transits changed into broader and shallower absorption structures, consistent with azimuthal spreading of the obscuring material. Our latest data obtained in 2022 and 2023 exhibits nearly no transit activity, apart from one single short transit detected on 2023 February 20. Such sharp transits are likely related to dust freshly released from a fragment either undergoing a collision with another solid body, or suffering structural stress due to tidal effects.

The long-term light curve of WD 1145+017 (Fig. 10) shows the system ≃0.1 mag fainter in the seasonal averages in the ASAS-SN *V*-band, which is within the limits of our offset calibration for that specific band. However, the ASAS-SN *V*-band data agrees well with the average ZTF *r*-band and ATLAS *c*-band data obtained in 2016 and 2017, suggesting that the drop in the ASAS-SN *V*-band brightness is real. This is somewhat puzzling, as the *K2* data presented by Vanderburg et al. (2015), obtained in the middle of

discovery of this system triggered a flurry of photometric (Gänsicke et al. 2016; Rappaport et al. 2016; Croll et al. 2017; Gary et al. 2017), spectroscopic (Xu et al. 2016; Hallakoun et al. 2017; Redfield et al. 2017; Izquierdo et al. 2018; Karjalainen et al. 2019; Fortin-Archambault et al. 2020), X-ray and polarimetric (Farihi et al. 2018), and theoretical (Gurri et al. 2017; Veras et al. 2017; Duvvuri, Redfield & Veras 2020) studies, providing very detailed insight into the morphology of the debris transits and into the physical processes occurring at WD 1145+017.

Gary et al. (2017) discussed the changes in transit activity of WD 1145+017, based on intense photometric monitoring of the

Figure 9. TNT light curves of WD 1145+017 obtained from 2016 to 2023 illustrate the large variation in the transit activity of the system, see Fig. 8 for detailed monitoring of the orbital averaged transmission throughout the same time span. Most of the light curves displayed here cover the dominant 4.49 h orbital period of the debris. The median values of the photometric uncertainties are illustrated by the error bar in the bottom-right of each panel.

the ASAS-SN *V*-band survey, caught the system in a state of low transit activity, and the increase in activity was only recorded shortly after the *K2* observations (e.g. Gänsicke et al. 2016; Rappaport et al. 2016). However, the calibration of the offsets of the survey pass-bands is colour dependent, so it is possible that WD 1145+017 might have changed both in brightness and/or colour around 2012 or 2013. As mentioned earlier, a small colour-dependence of the transit depths was found by Hallakoun et al. (2017). Whereas the observed amplitude of that colour dependence is insufficient to explain the long-term trend discussed above, our current insight into

the evolution of the debris transits is insufficient to rule out larger colour variations at certain epochs.

The period 2016 to 2023 is covered by multiple photometric surveys, and the seasonal averages agree well. All the survey data indicates that the system has been brightening by $\simeq 0.1$ mag from 2017 to 2023, which is consistent with the decrease of the transit activity, and the increase of the average orbital transmission discussed above.

TESS observations of WD 1145+017 were obtained in Sector 46 between 2021 December 4 to December 31. We retrieved the *TESS* short-cadence (20 s) pre-search data conditioning simple aperture
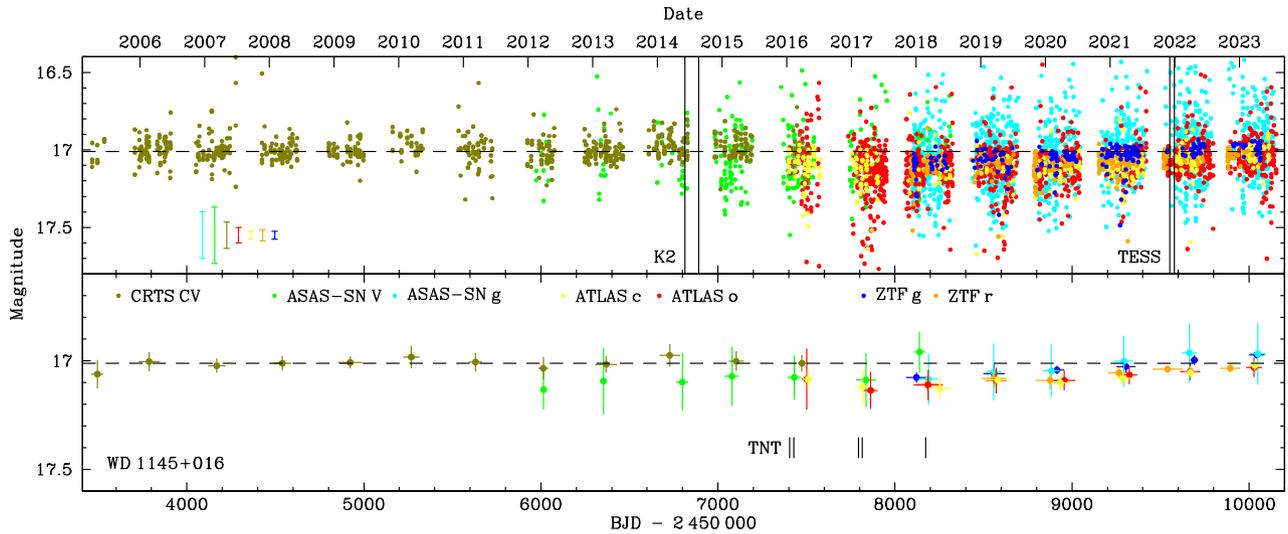
Figure 10. Long-term light curve of WD 1145+017, all symbols have the same meaning as in Fig. 2. We have used WD J093204.05+285044.61 as reference star to compute offsets between the different surveys. The *K2* observations that led to the discovery of the debris transits in WD 1145+017 were obtained in between the two vertical lines shown in the top panel. That period has only been covered by relatively sparse ASAS-SN *V*-band observations; however, a steady brightening of the system is seen in the seasonal data of the ASAS-SN *g*-band as well as in both bands of ZTF and ATLAS. This is consistent with the increase of the average transmission measured from detailed time-series photometry of the system, see Fig. 8. *TESS* observations were obtained during a quiescent period (see the last two panels of Fig. 9).
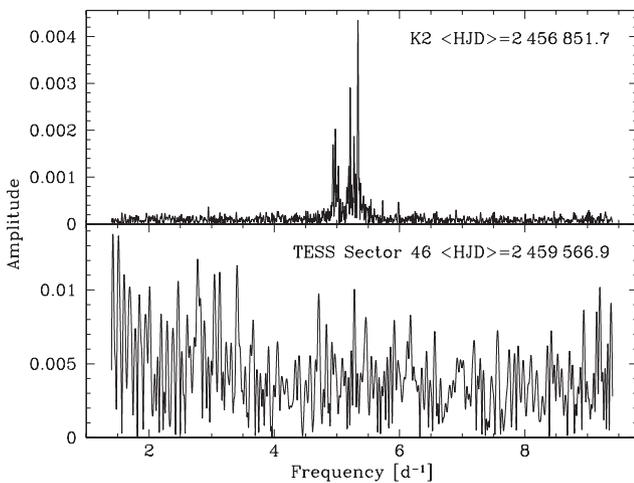
Figure 11. Amplitude spectra computed from the *K2* and *TESS* Sector 46 observations, the mean HJD epochs of the two data sets are labelled. To compare the two data sets, we normalized the light curves to a median flux of one prior to computing the amplitude spectra. The *K2* data clearly reveals the periodic transit signals identified by Vanderburg et al. (2015), which are not present in the *TESS* observations.

(PDCSAP) fluxes, as well as the *K2* PDCSAP fluxes, and computed discrete Fourier transforms for both data sets. A detailed comparison of the transit detection efficiency of the two data sets is difficult, as they were taken with different aperture sizes (*K2*: 0.95 m, *TESS*: 0.11 m), cadences (*K2*: 29.4 min, *TESS*: 20 s), and total baselines (*K2*: 80 d, *TESS*: 25.7 d). The crowding in *TESS* is not very severe, WD 1145+017 has a CROWDSAP value of 0.93 in Sector 46, suggesting that only about seven per cent of the flux in the aperture is not coming from the white dwarf. This has been incorporated in the relative fluxes in the PDCSAP *TESS* light curve. As a simple approach, we computed the amplitude spectra of the *K2* and *TESS*

data after normalizing both light curves to a median flux of one. Whereas the amplitude spectrum of the *K2* data clearly shows the multiple transit signals identified by Vanderburg et al. (2015), they are not detected in the *TESS* data (Fig. 11). This non-detection of a periodic signal in the *TESS* data is consistent with very weak or absent transits in the TNT light curves obtained in 2022 and 2023 (Fig. 9).

4 DISCUSSION

We detect long-term variations in the brightness of three white dwarfs exhibiting transiting debris: ZTF J0328−1219, ZTF J0923+4236, and WD 1145+017. Taking the average of the CRTS and ASAS-SN *V*-band data, ZTF J0328−1219 faded by ≃0.3 mag around 2012 to 2014 and has not yet fully recovered to the brightness level recorded by the earliest CRTS data. This might suggest that the system underwent a large collisional event around 2011, resulting in the production of large amounts of dust occulting the white dwarf, which has since then gradually dispersed, though leaving sufficient material to account for the ongoing transit activity, which implies continued dust production.

Similarly, WD 1145+017 exhibits an overall drop in its brightness, which concurs with a large increase in transit activity, followed by a subsequent gradual re-brightening. In the case of WD 1145+017, the long-term variations seen in the photometric survey data is accompanied by very detailed time-series photometry, corroborating that the overall trends seen in the brightness of WD 1145+017 are linked to varying amounts of transit activity.

The most puzzling case is that of ZTF J0923+4236, which exhibits deep aperiodic fading events over the past 17 years and large changes in the level of short-term variability, which appears to anti-correlate with the overall brightness of the system.

These long-term changes may be the result of the ongoing disruption of a planetesimal, or the collision between multiple fragments,

both leading to a temporarily increased dust production. Such an increased amount of dust production may result in a brightening at infrared wavelengths, as has been observed in WD 0145+234 (Wang et al. 2019).

Searching for photometric transit signals at white dwarfs is a very active research field (e.g. Faedi et al. 2011; Fulton et al. 2014; Belardi et al. 2016; Sandhaus et al. 2016; Dame et al. 2019), resulting, however, so far in very few detections: currently, only eight white dwarfs are known, or suspected to exhibit transits from planetary debris (Vanderburg et al. 2015; Guidry et al. 2020; Vanderbosch et al. 2020; Farihi et al. 2022). However, it is now clear that these searches will be affected by variations in transit activity – WD 1145+017 in its current state would be very unlikely to be identified from ground-based time-series photometry (Figs 8 and 9, bottom-right two panels).

This makes an assessment of the frequency of white dwarfs hosting disintegrating planetesimals difficult. van Sluijs & Van Eylen (2017) analysed the light curves of 1148 white dwarfs observed by *Kepler/K2* for transit signals, and did not discovery any system containing a disintegrating planetesimal beyond WD 1145+017 (Vanderburg et al. 2015). The *Kepler/K2* white dwarf sample is a random mix drawn from the literature, broadly speaking, magnitude limited, biased towards younger, brighter systems, and hence spanning a wide range of distances (WD 1145+017 is at $d \simeq 145$ pc, Gaia Collaboration et al. 2020), and it implies an detection rate of debris transits of $\simeq 1/1000$. Among the eight confirmed and candidate systems with debris transits, one is within 40 pc (WD 1054−226, $d = 36$ pc, Farihi et al. 2022), and considering that there are $\simeq 1000$ white dwarfs within 40 pc (McCleery et al. 2020; Tremblay et al. 2020; O'Brien et al. 2023) again suggests a rate of $\simeq 1/1000$; however, the 40 pc sample has not yet been homogeneously surveyed for transit signals. The closest white dwarf exhibiting debris transits reported by Guidry et al. (2020) is ZTF J0328−1219 ($d = 43$ pc), just slightly outside the 40 pc sample. Guidry et al. (2020) applied a temperature cut of 7000–16 000 K in their analysis, as well as astrometric and photometric quality cuts, which reduced the number of white dwarfs in their analysis with $d \lesssim 40$ pc to $\simeq 450$ – of which only about half have ZTF light curves, suggesting a detection rate of $\simeq 1/200$.

The details of the observational biases in the *Kepler/K2*, 40 pc, and Guidry et al. (2020) samples are difficult to quantify and compare, even more so as the case of WD1145+017 demonstrates that the strength of photometric transit signals can strongly vary on time-scales of years. Nevertheless, these three independent estimates, crude as they are, suggest that white dwarfs with detectable debris transits are not exceedingly rare. Factoring in that the detection implies a highly aligned orbital inclination, the true number of white dwarfs hosting planetesimals that are currently disintegrating is factors of several tens higher. It is hence conceivable that the fraction of white dwarfs with close-in debris undergoing disintegration is within factors of ten to a few of the fraction of white dwarfs exhibiting photospheric metals, which is $\simeq 25$ per cent of all white dwarfs, and the unmistakable signature of ongoing or recent accretion (Zuckerman et al. 2003, 2010; Koester et al. 2014). With only eight confirmed and candidate systems, it is still too early to gauge whether the intrinsic fraction of these systems among all white dwarfs might correlate with their effective temperatures, and hence cooling ages and/or their masses.

Extending the same reasoning to the transiting planet candidate at WD 1856+534 with $d \simeq 25$ pc (Vanderburg et al. 2020) results in a detection rate of $\sim 1/250$, which, again because of the need for a closely aligned viewing geometry, is highly underestimating the true number of white dwarfs with planets on close-in orbits. Other relatively nearby white dwarfs with subtle photometric or spectroscopic potential signatures of non-transiting planets (GD 394 at $d \simeq 50$ pc Dupuis et al. 2000; Wilson et al. 2019; Wilson, Hermes & Gänsicke 2020; GD 356 at $d \simeq 20$ pc, Li, Ferrario & Wickramasinghe 1998; Gänsicke et al. 2020; WD J122619.77+183634.46 at $\simeq 36$ pc, Manser et al. 2023, and WD J041246.84+754942.26 at $d \simeq 35$ pc and WD J165335.21−100116.33 at $d \simeq 33$ pc, Elms et al. 2023) corroborate the hypothesis that these systems might be relatively common.

5 CONCLUSIONS

We detect long-term variability in three white dwarfs that are known to exhibit transits from planetary debris, and at least in two cases, the long-term changes in brightness correlate with the level of activity detected in high-speed photometry on a time-scale of several hours. Our study highlights the potential of a joint analysis of the nearly two decades of large-area survey photometry as a novel approach in identifying white dwarfs that exhibit irregular variability. The scientific potential of future time-domain surveys would benefit from (quasi)simultaneous multiband photometry to probe for changes in brightness and colour. Based on crude, but independent estimates, we suggest that debris transits may be detectable among one in a few hundred white dwarfs, and that it is likely that a significant fraction of all white dwarfs exhibiting photospheric metals currently host disintegrating planetesimals.

institutes, the Max Planck Institute for Astronomy, Heidelberg, and the Max Planck Institute for Extraterrestrial Physics, Garching, the Johns Hopkins University, Durham University, the University of Edinburgh, the Queen's University Belfast, the Harvard-Smithsonian Center for Astrophysics, the Las Cumbres Observatory Global Telescope Network Incorporated, the National Central University of Taiwan, the Space Telescope Science Institute, the National Aeronautics and Space Administration under Grant No. NNX08AR22G issued through the Planetary Science Division of the NASA Science Mission Directorate, the National Science Foundation Grant No. AST-1238877, the University of Maryland, Eotvos Lorand University (ELTE), the Los Alamos National Laboratory, and the Gordon and Betty Moore Foundation. This paper includes data collected by the Kepler mission and obtained from the MAST data archive at the Space Telescope Science Institute (STScI). Funding for the Kepler mission is provided by the NASA Science Mission Directorate. STScI is operated by the Association of Universities for Research in Astronomy, Inc., under NASA contract NAS 5-26555. This paper includes data collected by the TESS mission, which are publicly available from the Mikulski Archive for Space Telescopes (MAST). Funding for the TESS mission is provided by NASA's Science Mission directorate.

DATA AVAILABILITY

The ASAS-SN, ATLAS, and ZTF light curves can be retrieved from the respective archives, and we will make the CRTS and TNT light curves available upon reasonable requests communicated to the lead author.

REFERENCES

Adams F. C., Anderson K. R., Bloch A. M., 2013, MNRAS, 432, 438
Antoniadou K. I., Veras D., 2019, A&A, 629, A126
Belardi C., Kilic M., Munn J. A., Giannias A., Barber S. D., Dey A., Stetson P. B., 2016, MNRAS, 462, 2506
Bellm E. C. et al., 2019, PASP, 131, 018002
Bertin E., Arnouts S., 1996, A&AS, 117, 393
Bonsor A., Wyatt M. C., 2012, MNRAS, 420, 2990
Brown J. C., Veras D., Gänsicke B. T., 2017, MNRAS, 468, 1575
Caiazzo I., Heyl J. S., 2017, MNRAS, 469, 2750
Chambers K. C. et al., 2016, preprint (arXiv:1612.05560)
Croll B. et al., 2017, ApJ, 836, 82
Cunningham T. et al., 2021, MNRAS, 503, 1646
Dame K., Belardi C., Kilic M., Rest A., Giannias A., Barber S., Brown W. R., 2019, MNRAS, 490, 1066
Debes J. H., Sigurdsson S., 2002, ApJ, 572, 556
Debes J. H., Kilic M., Faedi F., Shkolnik E. L., Lopez-Morales M., Weinberger A. J., Slesnick C., West R. G., 2012, ApJ, 754, 59
Dennihy E., Clemens J. C., Dunlap B. H., Fanale S. M., Fuchs J. T., Hermes J. J., 2018, ApJ, 854, 40
Dhillon V. S. et al., 2014, MNRAS, 444, 4009
Drake A. J. et al., 2009, ApJ, 696, 870
Dupuis J., Chayer P., Vennes S., Christian D. J., Kruk J. W., 2000, ApJ, 537, 977
Duvvuri G. M., Redfield S., Veras D., 2020, ApJ, 893, 166
Elms A. K. et al., 2023, MNRAS, 524, 4996
Faedi F., West R. G., Burleigh M. R., Goad M. R., Hebb L., 2011, MNRAS, 410, 899
Farihi J. et al., 2018, MNRAS, 474, 947
Farihi J. et al., 2022, MNRAS, 511, 1647
Fortin-Archambault M., Dufour P., Xu S., 2020, ApJ, 888, 47
Frewen S. F. N., Hansen B. M. S., 2014, MNRAS, 439, 2442
Fulton B. J. et al., 2014, ApJ, 796, 114
Gaia Collaboration et al., 2020, A&A, 649, A1

Gänsicke B. T., Araujo-Betancor S., Hagen H.-J., Harlaftis E. T., Kitsionas S., Dreizler S., Engels D., 2004, A&A, 418, 265
Gänsicke B. T., Marsh T. R., Southworth J., Rebassa-Mansergas A., 2006, Science, 314, 1908
Gänsicke B. T. et al., 2016, ApJ, 818, L7
Gänsicke B. T., Koester D., Farihi J., Toloza O., 2018, MNRAS, 481, 4323
Gänsicke B. T., Schreiber M. R., Toloza O., Fusillo N. P. G., Koester D., Manser C. J., 2019, Nat, 576, 61
Gänsicke B. T., Rodríguez-Gil P., Gentile Fusillo N. P., Inight K., Schreiber M. R., Pala A. F., Tremblay P.-E., 2020, MNRAS, 499, 2564
Gary B. L., Rappaport S., Kaye T. G., Alonso R., Hambschs F.-J., 2017, MNRAS, 465, 3267
Gentile Fusillo N. P. et al., 2021, MNRAS, 504, 2707
Girven J., Brinkworth C. S., Farihi J., Gänsicke B. T., Hoard D. W., Marsh T. R., Koester D., 2012, ApJ, 749, 154
Guidry J. A. et al., 2020, ApJ, 912, 125
Gurri P., Veras D., Gänsicke B. T., 2017, MNRAS, 464, 321
Hallakoun N. et al., 2017, MNRAS, 469, 3213
Izquierdo P. et al., 2018, MNRAS, 481, 703
Jura M., 2003, ApJ, 584, L91
Karjalainen M., de Mooij E. J. W., Karjalainen R., Gibson N. P., 2019, MNRAS, 482, 999
Kenyon S. J., Bromley B. C., 2017a, ApJ, 844, 116
Kenyon S. J., Bromley B. C., 2017b, ApJ, 850, 50
Kochanek C. S. et al., 2017, PASP, 129, 104502
Koester D., Gänsicke B. T., Farihi J., 2014, A&A, 566, A34
Larson S., Beshore E., Hill R., Christensen E., McLean D., Kolar S., McNaught R., Garradd G., 2003, in AAS/Division for Planetary Sciences Meeting Abstracts #35. p. 36.04
Li J., Ferrario L., Wickramasinghe D., 1998, ApJ, 503, L151
Malamud U., Perets H. B., 2020a, MNRAS, 492, 5561
Malamud U., Perets H. B., 2020b, MNRAS, 493, 698
Maldonado R. F., Villaver E., Mustill A. J., Chávez M., Bertone E., 2021, MNRAS, 501, L43
Manser C. J. et al., 2016, MNRAS, 455, 4467
Manser C. J. et al., 2019, Science, 364, 66
Manser C. J. et al., 2023, MNRAS, 521, 4976
Martin R. G., Livio M., Smallwood J. L., Chen C., 2020, MNRAS, 494, L17
Masci F. J. et al., 2019, PASP, 131, 018003
McCleery J. et al., 2020, MNRAS, 499, 1890
Metzger B. D., Rafikov R. R., Bochkarev K. V., 2012, MNRAS, 423, 505
Miranda R., Rafikov R. R., 2018, ApJ, 857, 135
Mustill A. J., Villaver E., 2012, ApJ, 761, 121
Mustill A. J., Villaver E., Veras D., Gänsicke B. T., Bonsor A., 2018, MNRAS, 476, 3939
O'Brien M. W. et al., 2023, MNRAS, 518, 3055
Payne M. J., Veras D., Holman M. J., Gänsicke B. T., 2016, MNRAS, 457, 217
Rappaport S., Gary B. L., Kaye T., Vanderburg A., Croll B., Benni P., Foote J., 2016, MNRAS, 458, 3904
Rappaport S., Gary B. L., Vanderburg A., Xu S., Pooley D., Mukai K., 2018, MNRAS, 474, 933
Redfield S., Farihi J., Cauley P. W., Parsons S. G., Gänsicke B. T., Duvvuri G. M., 2017, ApJ, 839, 42
Rodrigo C., Solano E., 2020, in XIV.0 Scientific Meeting (virtual) of the Spanish Astronomical Society. p. 182
Sackmann I.-J., Boothroyd A. I., Kraemer K. E., 1993, ApJ, 418, 457
Sandhaus P. H., Debes J. H., Ely J., Hines D. C., Bourque M., 2016, ApJ, 823, 49
Schreiber M. R., Gänsicke B. T., Toloza O., Hernandez M.-S., Lagos F., 2019, ApJ, 887, L4
Schwarzenberg-Czerny A., 1996, ApJ, 460, L107
Shappee B. J. et al., 2014, ApJ, 788, 48
Shestakova L. I., Serebryanskiy A. V., 2023, MNRAS, 524, 4506
Smallwood J. L., Martin R. G., Livio M., Lubow S. H., 2018, MNRAS, 480, 57
Smith K. W. et al., 2020, PASP, 132, 085002

Stephan A. P., Naoz S., Zuckerman B., 2017, ApJ, 844, L16

Swan A., Farihi J., Wilson T. G., 2019, MNRAS, 484, L109

Swan A., Farihi J., Wilson T. G., Parsons S. G., 2020, MNRAS, 496, 5233

Tonry J. L. et al., 2018, PASP, 130, 064505

Tremblay P. E. et al., 2020, MNRAS, 497, 130

van Sluijs L., Van Eylen V., 2017, MNRAS, 474, 4603

Vanderbosch Z. et al., 2020, ApJ, 897, 171

Vanderbosch Z. P. et al., 2021, ApJ, 917, 41

Vanderburg A. et al., 2015, Nat, 526, 546

Vanderburg A. et al., 2020, Nat, 585, 363

Veras D., Leinhardt Z. M., Bonsor A., Gänsicke B. T., 2014a, MNRAS, 445, 2244

Veras D., Shannon A., Gänsicke B. T., 2014b, MNRAS, 445, 4175

Veras D., Leinhardt Z. M., Eggl S., Gänsicke B. T., 2015, MNRAS, 451, 3453

Veras D., Carter P. J., Leinhardt Z. M., Gänsicke B. T., 2017, MNRAS, 465, 1008

Veras D., McDonald C. H., Makarov V. V., 2020, MNRAS, 492, 5291

Wang T.-g. et al., 2019, ApJ, 886, L5

Wilson D. J., Gänsicke B. T., Koester D., Raddi R., Breedt E., Southworth J., Parsons S. G., 2014, MNRAS, 445, 1878

Wilson D. J. et al., 2019, MNRAS, 483, 2941

Wilson D. J., Hermes J. J., Gänsicke B. T., 2020, ApJ, 897, L31

Xu S., Jura M., 2014, ApJ, 792, L39

Xu S., Jura M., Dufour P., Zuckerman B., 2016, ApJ, 816, L22

Xu S. et al., 2018a, MNRAS, 474, 4795

Xu S. et al., 2018b, ApJ, 866, 108

Xu S. et al., 2019, AJ, 157, 255

Zhou G. et al., 2016, MNRAS, 463, 4422

Zuckerman B., Becklin E. E., 1987, Nat, 330, 138

Zuckerman B., Koester D., Reid I. N., Hünsch M., 2003, ApJ, 596, 477

Zuckerman B., Melis C., Klein B., Koester D., Jura M., 2010, ApJ, 722, 725

This paper has been typeset from a TEX/LATEX file prepared by the author.